Geoelectric surveys in the southern part of the Yangsan Fault

Kiehwa Lee · Won-Seok Han

Department of Geological Sciences, Seoul National University

ABSTRACT

In order to delineate the geoelectric structures of the Yangsan Fault in the Kyeongsang Basin, geoelectric surveys were conducted on two separate areas in the southeastern part of the Korean Peninsula; one between Ijo-ri, Kyeongju and Seoha-ri, Ulsan, and the other between Samgam-ri and Heuisan-ri, Yangsan. The fault zone is well indicated by low resistivity values and the weathered layer in the fault zone turns out to get thicker from north to south in these areas. The weathered layer extends down to a depth of about 100 m near Seoha-ri and Heuisan-ri, and to about 50-70 m in other places. The range of resistivity for the weathered layer of the fault zone is 40-300 Ωm, except near Heuisan-ri where very low resistivity of about 10 Ωm was obtained. It appears that there exists a systematic variation in depth to the unweathered basements along the Yangsan Fault. Horizontal mappings show that apparent resistivities decrease towards the Yangsan Fault

Key words: geoelectric survey, electrical resistivity, Yangsan Fault, fault zone

요 약

한반도 남동부 경상분지에 위치한 양산단층의 지전기학적 구조를 밝히기 위하여 경주시 이조리와 울산시 서하리, 양산시 삼감리와 회산리 사이에서 전기비저항 탐사를 수행하였다. 단층파쇄대는 낮은 전기비저항값을 가지며 단층파쇄대에 분포하는 풍화대는 남쪽으로 향할수록 두꺼워지는 것으로 나타났다. 풍화대의 깊이는 서하리와 회산리에서 약 100 m 이며 다른 지역에서는 약 50-70 m 정도이다. 단층파쇄대에 위치하는 풍화대의 전기비저항값은 회산리에서 얻어진 약 10 Ωm의 매우 낮은 값을 제외하고는 약 40-300 Ωm 정도이다. 연구지역 내에서는 풍화대 하부에 위치하는 기반암의 깊이가 양산단층을 따라 남쪽으로 향할수록 깊어지는 특징적인 변화 양상을 갖는 것으로 보인다. 수평탐사 결과는 양산단층에 가까워질수록 겉보기 비저항값이 감소함을 보여준다

주요어: 지전기탐사, 전기비저항, 양산단층, 단층파쇄대

(Lee, Kiehwa and Han, Won-Seok, Department of Geological Sciences, Seoul National University, Shillim-Dong, Kwanak-Gu, Seoul, 151-742, Korea. email: kihwalee@plaza.snu.ac.kr)

1. INTRODUCTION

The Yangsan Fault and its subsidiary faults such as Dongrae, Eonyang, Ulsan, and Ilkwang Faults are situated within the Kyeongsang Basin in the southeastern part of the Korean Peninsula (Fig. 1). They constitute the Yangsan Fault System which is believed to have initiated from the Bulgugsa
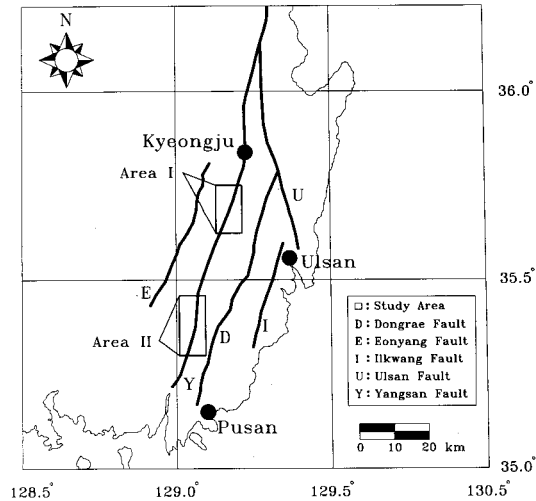
Fig. 1. Map showing locations of the study areas and major faults of the Yangsan Fault System.

Orogeny (Kang, 1981). Recent seismological studies suggest that Yangsan Fault System is seismologically active (Lee · Na, 1983; Lee · Jin, 1991).

It is believed that the fault zone is sheared and possibly saturated with consequently reduced resistivities (Olorunfemi *et al.*, 1986). Therefore, geoelectric methods can be effectively utilized to investigate the fault zone. A number of geoelectric studies on the geoelectric characteristics of the Yangsan Fault System have been carried out since the early 1980s (Kim · Kim, 1983; Lee *et al.*, 1985, 1992; Kim · Lee, 1987, 1988; Kim *et al.*, 1990; Lee · Um, 1992; Lee · Lee, 1997). These studies revealed horizontal and vertical resistivity structure of the fault zone.

Study areas are located along the (inferred) Yangsan Fault (Fig. 1). In these areas, 43 Schlumberger vertical electric soundings (VES) and four Wenner mappings were conducted. Previous geoelectric studies in these areas were mainly concerned in delineating the horizontal extent of the fault zone. In this study, however, an emphasis will be placed on the vertical structure of fault zone, instead.

According to Kim · Lee (1988), the Yangsan Fault strikes NNE and has a nearly vertical dip. A vertical fault can be more effectively studied with VES conducted along the fault and horizontal mappings across it. In this study, VES and horizontal mappings were carried out parallel and perpendicular to the inferred fault, respectively, as much as possible.

2. GEOLOGY

Geoelectric studies were conducted on two separate areas; one is between Ijo-ri, Kyeongju and Seoha-ri, Ulsan (Area I), and the other between Samgam-ri and Heuisan-ri, Yangsan (Area II). These two areas are taken since they lie in the proposed central and southern segments of the Yangsan Fault (Lee · Jin, 1991) whose electrical structures are not fully understood. Both areas suffered several episodes of intrusion and extrusion of igneous rocks during the Late Cretaceous, and are characterized by concentration of lineaments, especially of NNE trend (Kim · Lee, 1987, 1988).

Area I is located in the proposed central segment of the Yangsan Fault. This area consists of Cretaceous sedimentary rocks of the Daegu Formation, intrusive or extrusive andesitic volcanic rocks, and igneous rocks of Cretaceous age (Lee · Lee, 1972) (Fig. 2). The Daegu Formation and Cretaceous andesite cover most of the area and several faults having NNE and NS strikes are recognized in the area (Kim *et al.*, 1971). Igneous rocks of the Late Cretaceous Eonyang granite intrude sedimentary and volcanic rocks. Most of the Eonyang granites are biotite granites. Quaternary alluvium located in northern part of this area develops along the Hyungsan River.

Area II lies in the southern segment of the Yangsan Fault, and its geology generally corresponds to the upper part of the Kyeongsang System (Lee · Kang, 1964). The Daeyangdong Formation of Early Cretaceous Hayang Group; chert, felsophyre, and feldspar porphyry of Middle Cretaceous Yucheon Group; and igneous rocks of Late Cretaceous Bulgugsa Granitic Rocks are distributed in this area (Fig. 3). The Daeyangdong
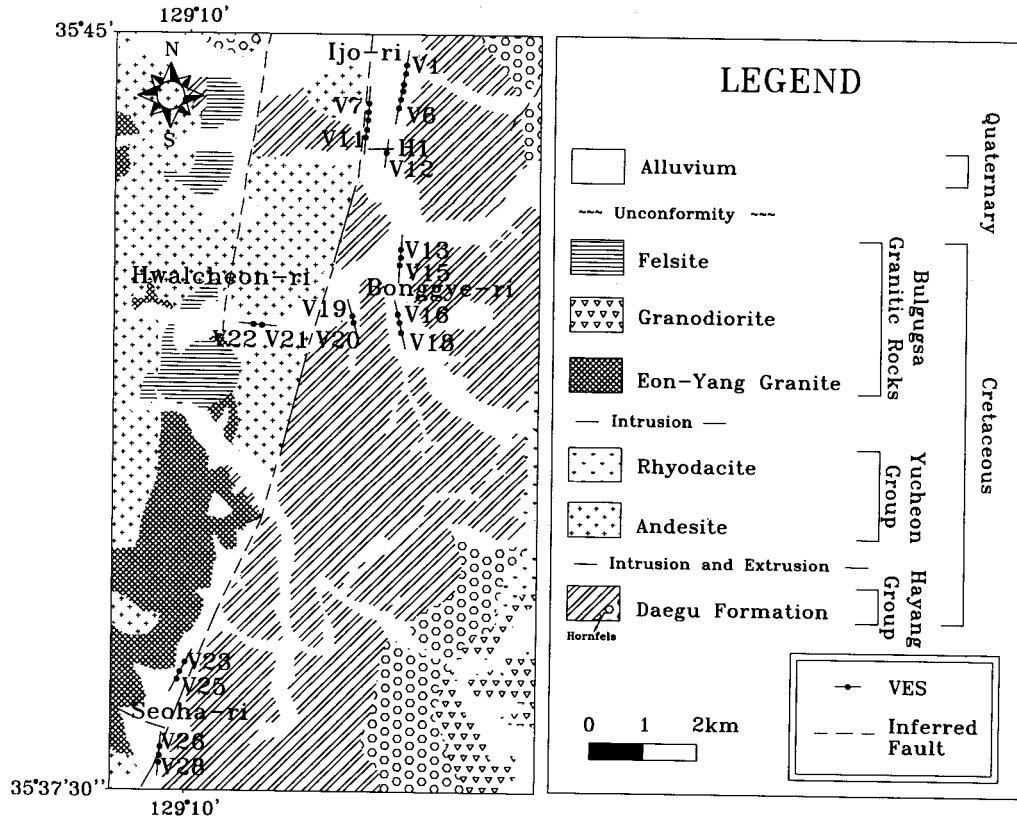
Fig. 2. Geological map showing locations of VES points and horizontal survey line of Area I (after Kim *et al.*, 1971).

Formation consisting mainly of purple shale is the oldest rocks in this area and suffered the late volcanic activities of the andesitic rocks. The members of Yucheon Group are intruded by acidic plutonic and hypabyssal rocks of Bulgugsa Granitic Rocks. Biotite granite (the Eonyang granite of Area I) which is widely distributed in the Kyeongsang Basin is the most abundant igneous rock type of Bulgugsa Granitic Rocks (Son *et al.*, 1978). Quaternary alluvium consisting of clay, sand, and gravel develops along the Yangsan Stream. Geology of the eastern part of the Yangsan Fault differs from that of the western part (Lee · Kang, 1964). Directions of intrusion or extrusion of igneous rocks in both parts are different from each

other and identical rock bodies are cut by the Yangsan Fault. The Daeyangdong Formation and Chusan andesitic rocks are cut by a number of faults.

3. ELECTRIC SURVEY

In order to investigate the geoelectric structure of the Yangsan Fault in the study areas, 43 Schlumberger VES and four Wenner mappings were conducted (Figs. 2 and 3) with ABEM Terrameter SAS 300B. The maximum distance between current electrodes in VES was about 430 m, and electrode separation for horizontal mappings 30 m.
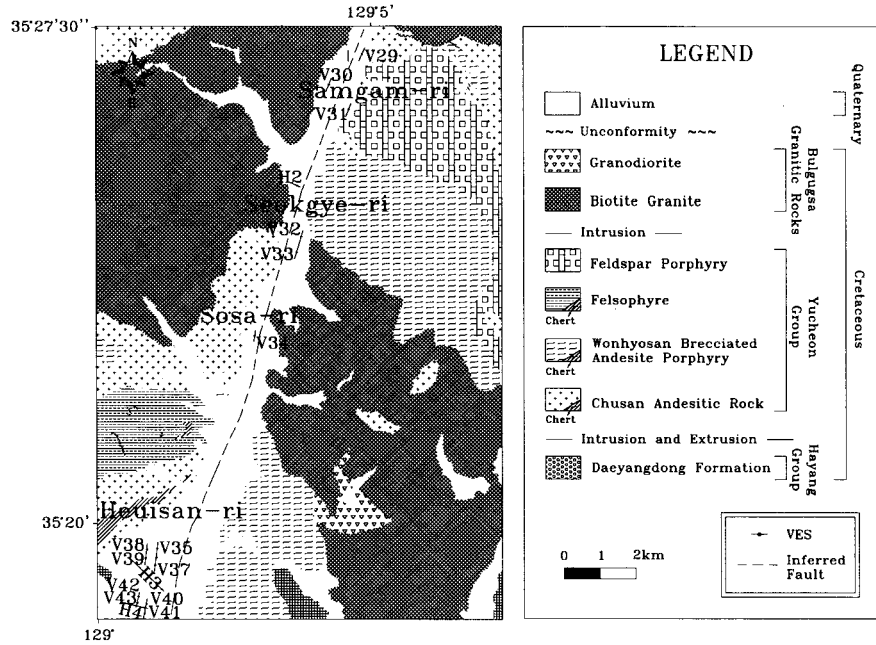
Fig. 3. Geological map showing locations of VES points and horizontal survey lines of Area II (after Lee · Kang, 1964).
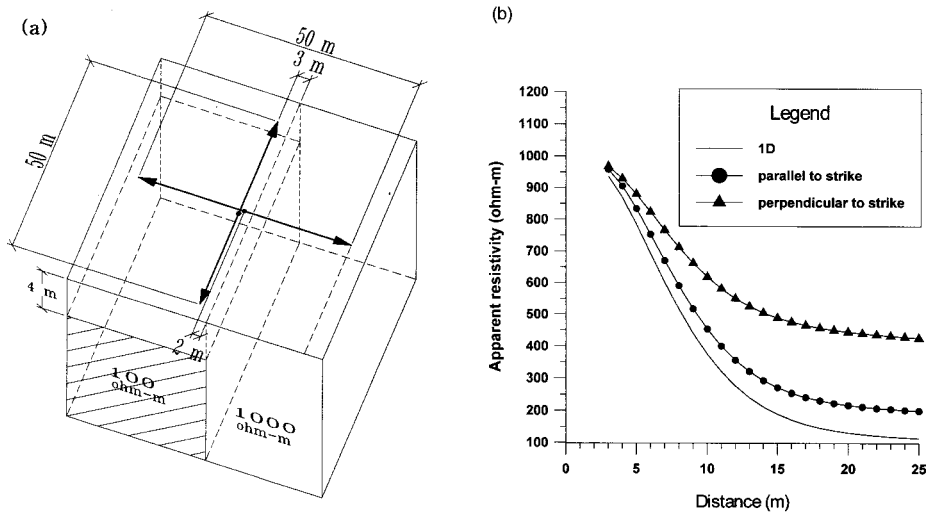

Fig. 4. Numerical simulation of Schlumberger VES on a vertical fault zone; (a) vertical fault zone model and two Schlumberger VES profiles with different directions, (b) apparent resistivity curves for both 3-D (solid triangle: perpendicular to strike, solid circle: parallel to strike) and 1-D (solid line) models.

In case of a nearly vertical fault like the Yangsan Fault, the fault zone can be modeled with a composite of infinitely long prisms of finite width and thickness in the strike direction. However, we carried out Schlumberger VES assuming one-dimensional subsurface structure. Under the circumstances, the direction of VES will affect the apparent resistivity. In order to find the VES direction that best portrays two-dimensional resistivity structure in the Schlumberger array, a numerical simulation was carried out (Fig. 4). Fig. 4a shows part of vertical fault model with two different VES directions, one perpendicular to the strike of fault and the other parallel to it. The fault zone of 100 ohm-m is modeled as a two dimensional structure with infinite thickness. The maximum distance between current electrodes is set to be 50 m, and VES points are two and three meters apart from surface projection of the flank of fault zone for arrays perpendicular and parallel to the strike, respectively. Even though this model is two-dimensional, three-dimensional resistivity modeling is required since one profile is parallel to the strike.

A finite-difference technique (Dey · Morrison, 1979; Lee · Yoon, 1997) was employed to calculate the potential distribution due to a point current source on the surface of half-space with an arbitrary 3-dimensional distribution of conductivity. The results of calculation are shown in Fig. 4b Solid circles and triangles represent apparent resistivity values for profiles parallel and perpendicular to the strike, respectively. And the solid curve represents apparent resistivity for one-dimensional two layered structure. The resistivity and thickness of the first layer are 1,000 ohm-m and 4 m, respectively, and resistivity of the bottom half space is 100 ohm-m. Fig. 4b clearly shows that the parallel array portrays one-dimensional structure better than the perpendicular array. Therefore, it can be concluded that Schlumberger VES array parallel to the strike is superior to perpendicular array in delineating two-dimensional resistivity structure.

Based on the above analysis, VES were conducted with electrodes parallel to the strike of fault as much as possible in this study. In horizontal mapping, however, electrodes were deployed perpendicular to the fault to clearly locate the discontinuity in the vicinity of the contact.

The inferred Yangsan Fault lies on the Kyeongbu Expressway, and there are rivers (or streams) where the field works were carried out. Topographic conditions prevented most of horizontal mappings traversing the fault trace.

4. INTERPRETATIONS

All VES data were analyzed using Zohdy's method (1989) that automatically interprets sounding data from apparent resistivity curve. In Zohdy's scheme, the number of layers in the interpreted model equals the number of digitized points on the sounding curve. The resulting multi-layer model, however, can be regarded as a set of several layers if adjacent layers have similar resistivity values. All VES data of the study area indicate that the resistivity structure of the area can be interpreted as a four-layer system. The resistivity decreases from the first layer to the third layer (Q-type), and then increases to the fourth layer (QH-type).

According to Ward (1990), the resistivity of fresh granite ranges from about 300 to 30,000 Ωm and that of weathered or altered granite from about 1 to 100 Ωm. The Yangsan Fault in the study area develops between granite and andesite. Thus, it seems reasonable to assume that the weathered layer in the fault zone extends down to a depth of about 300 Ωm which is the lower limit of resistivity of fresh granite. The resistivity range 10-300 Ωm of the third layer indicates this layer has experienced weathering or alteration. Therefore, the first-, second-, third-, and fourth-layer may be interpreted as top soil, alluvium, weathered layer, and basement, respectively. Although Area I and Area II are distant from each other, their geoelectric structures may be interpreted as a four-layer system. This suggests that fault zone generally develops along the Yangsan Fault and the

geoelectric method is efficient for delineating geological structure of the fault zone.

In the horizontal mapping of the fault zone, it is expected that apparent resistivity starts to decrease at the contact and maintains low value over the fault zone and increases away from the fault zone. In this study, however, this trend of apparent resistivity was not observed. It appears that the profile length is too short to leave the fault zone. Low apparent resistivities were obtained throughout the profile H4, and resistivity decreases toward the inferred fault were observed on profiles H1, H2, and H3.

4.1. VERTICAL SOUNDINGS

4.1.1. Area I

In Area I, 28 VES were carried out on four separate sites (Ijo-ri, Hwalcheon-ri, Bonggye-ri, and Seoha-ri) (Fig. 2).

In Ijo-ri 12 VES (V1-12) were conducted. All VES are on the eastern side of the inferred fault; VES V1-6 and V12 are on the eastern side of river, and VES V7-11 on the western side. Due to problems such as poor contact between electrodes and the ground surface, anomalous resistivity

bodies in the vicinity of electrodes, erratic VES data may be obtained which cannot be interpreted properly. In this case, however, if VES are taken quite close to each other, the resistivity structure of a region may be inferred from the results for the neighboring VES. In this regard, the spacing between adjacent VES was set as small as 150 m in this survey.

Figs. 5a and 5b show interpretations of VES V5 and V10, respectively. Apparent resistivity curves for VES V1-6 and V12 are similar in shape, resulting in similar interpretations. Apparent resistivity curves for VES V7-11 are somewhat different from those for VES V1-6 and V12; however, they have similar features. Amongst these soundings, VES V5 and V10 were chosen as representatives of VES V1-12. The resistivity of the weathered layer for VES V7-11 close to the inferred fault ranges from 30 to 200 Ωm, while that for VES V1-6 and V12 distant from the fault ranges from 50 to 300 Ωm. The depths to the basement for VES V1-12 are about 50 to 70 m. In conclusion, geological layers above the basement in the fault zone become slightly more conductive toward the inferred fault without significant change
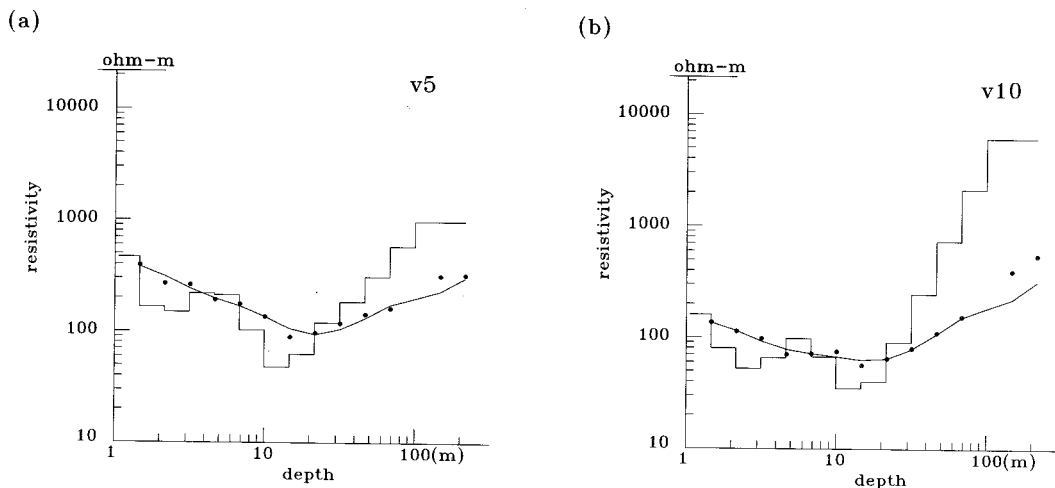

Fig. 5. Interpretation of Schlumberger VES at V5 and V10. Dots, curves, and solid lines denote field data, calculated apparent resistivity, and interpreted model, respectively: (a) V5, (b) V10.
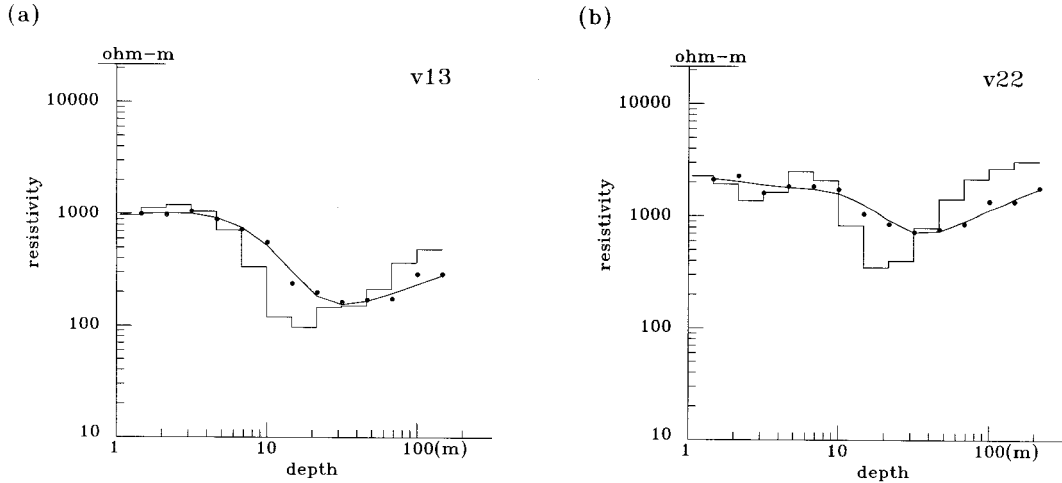
(a)   (b)

Fig. 6. Interpretation of Schlumberger VES at V13 and V22. Dots, curves, and solid lines denote field data, calculated apparent resistivity, and interpreted model, respectively: (a) V13, (b) V22.

in depth.

In Bonggye-ri soundings V13-15 were taken. Interpretations of VES V13-15 show similar resistivity structures. The depth to the basement and resistivity value of the weathered zone are about 50-70 m and 100-200 Ωm, respectively (Fig.

6a). This interpretation seems to indicate the fault zone extends horizontally to these localities.

In order to investigate the lateral extent of fault zone VES V16-18 and V19-20 were conducted south of VES V13-15. It is known that horizontal mapping is superior to VES in examining the
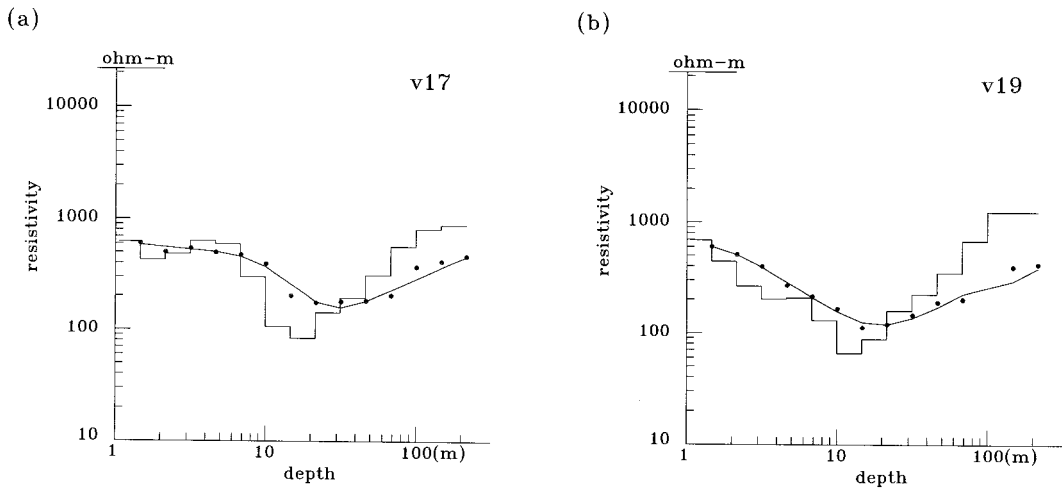
(a)   (b)

Fig. 7. Interpretation of Schlumberger VES at V17 and V19. Dots, curves, and solid lines denote field data, calculated apparent resistivity, and interpreted model, respectively: (a) V17, (b) V19.

lateral extent of the fault zone. However, it was impossible to carry out horizontal mapping from VES V16 to V19 due to topographic condition in this area. Thus, the lateral extent of the fault zone is inferred by horizontal variation of vertical resistivity structures from VES V16-18 and V19-20. Figs. 7a and 7b illustrate interpretations of VES V17 and V19, respectively; the weathered layer in this area has resistivity of 70-200 Ωm, and extends down to a depth of about 50 m. It can be seen in these figures the low resistivity layer of VES V19 which is closer to the fault trace than VES V17 is thicker than that of VES V17. The depths to basement for VES V17 and V19 are similar to those for VES V1-12. Therefore, it appears that fault zone extends eastward to locations of VES V16-18 about 1.5 km from the fault trace.

In Hwalcheon-ri VES V21-22 were conducted. Their locations are about 1 km west of the inferred fault. These two VES were carried out perpendicular to the fault trace. Interpretations of VES V21-22 show that the third layer of this area is similar to those of VES V1-20 in depth extent (about 50 m) but has higher resistivity of about

400-800 Ωm (Fig. 6b). This indicates that the fault zone of the western part of the inferred fault is poorly developed compared to the eastern part.

VES V23-28 were conducted in Seoha-ri located in the southern part of Area I. Fig. 8a shows that the weathered zone for VES V25 has resistivity of about 60-300 Ωm and reaches down to about 100 m from the surface. Interpretations of VES V26-28 are quiet different from those of VES V1-22 in depth extent. Fig. 8b shows that the weathered layer for VES V26 has resistivity of about 40-60 Ωm and extends down to over 100 m; the effect of basement is not observed. It appears that the weathered layer in the fault zone of this area develops more deeply than other areas, probably due to a subsidiary fault striking NW north of VES V26 (Fig. 2). Lee · Lee (1997) reported that the depth to the basement close to the southern part of Area I reaches to about 100 m. In conclusion, it appears that the weathered layer in the Yangsan Fault extends deeper from north to south in Area I.

4.1.2. Area II

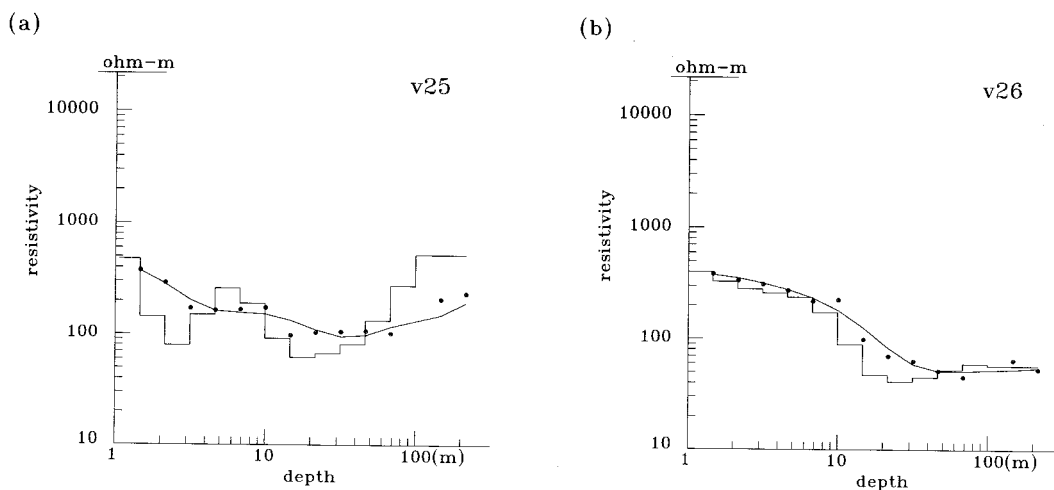In Area II, 15 VES were carried out in four

(a)

(b)

Fig. 8. Interpretation of Schlumberger VES at V25 and V26. Dots, curves, and solid lines denote field data, calculated apparent resistivity, and interpreted model, respectively: (a) V25, (b) V26.
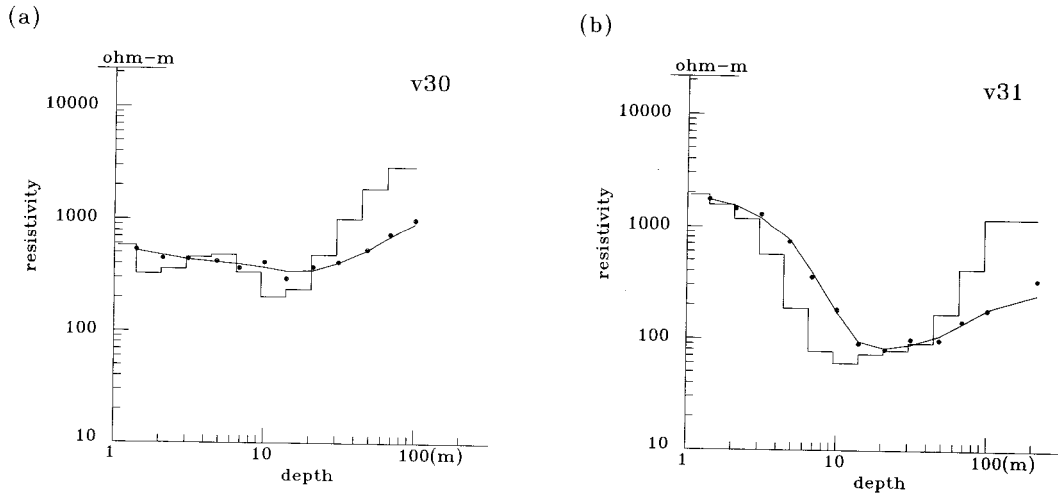
Fig. 9. Interpretation of Schlumberger VES at V30 and V31. Dots, curves, and solid lines denote field data, calculated apparent resistivity, and interpreted model, respectively: (a) V30, (b) V31.

separate sites (Samgam-ri, Seokgye-ri, Sosa-ri, and Heuisan-ri) (Fig. 3).

VES V29-31 were conducted in Samgam-ri. Interpreted structures of VES V29 and V31 conducted on the eastern side of the inferred fault are similar except for the resistivity value of the first layer. But the interpretation of VES V30 west of the inferred fault is different from those of VES V29 and V31. Figs. 9a and 9b illustrate interpretations of VES V30 and V31, respectively. The third layers of VES V30 and V31 extend down to depths of about 20 m and 60 m, respectively, and the third layer of VES V31 is more conductive than that of VES V30. Thus, it is
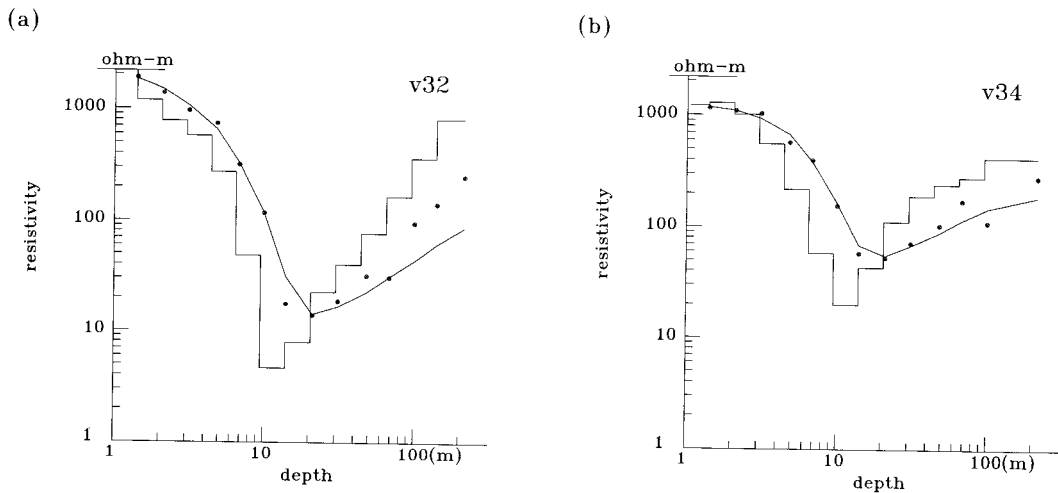

Fig. 10. Interpretation of Schlumberger VES at V32 and V34. Dots, curves, and solid lines denote field data, calculated apparent resistivity, and interpreted model, respectively: (a) V32, (b) V34.
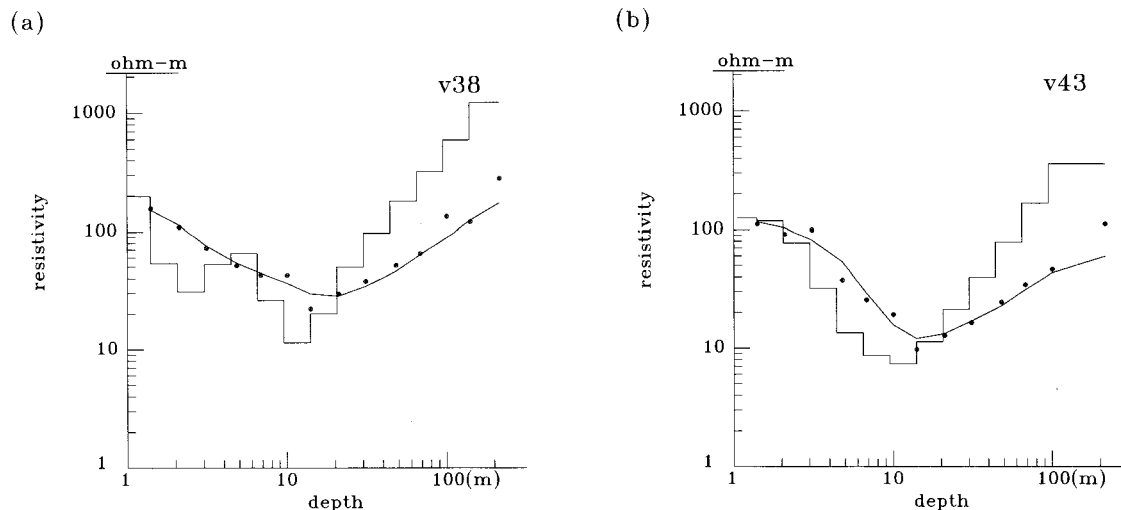
(a)

(b)

Fig. 11. Interpretation of Schlumberger VES at V38 and V43. Dots, curves, and solid lines denote field data, calculated apparent resistivity, and interpreted model, respectively: (a) V38, (b) V43.

inferred that weathered layer in the eastern part of the inferred fault is better developed than in the western part as Area I.

VES V32-43 were conducted south of Seokgye-ri. It is interpreted that the weathered layer of this area has low resistivity of about 10-200 Ωm and extends down to 90 to 100 m depth. The weathered layer of this area extends more deeply than other areas excluding Seoha-ri and is more conductive than other areas. This phenomenon may relate to the presence of the Nakdong River and the Yangsan Stream in the area.

Figs. 10a and 10b illustrate interpretations of VES V32 and V34 conducted in Seokgye-ri and Sosa-ri, respectively. Interpretation of VES V32 which is similar to that of VES V33 shows a very conductive zone extending to about 90-100 m depth. Interpretation of VES V34 indicates that the low resistivity zone has resistivity of 20-300 Ωm and extends down to about 100 m depth.

VES V35-43 were conducted in Heuisan-ri. It is interpreted that the weathered layers for VES V40-43 in the vicinity of the Nakdong River are slightly more conductive than those for VES V35-39. Depths to the basement for VES V35-43

are about 90-100 m. Fig. 11a and 11b illustrate interpretations of VES V38 and V43, respectively. A similarity between resistivity structures of VES V35-39 and those of VES V40-43 is observed. This seems to vindicate the assumption of one-
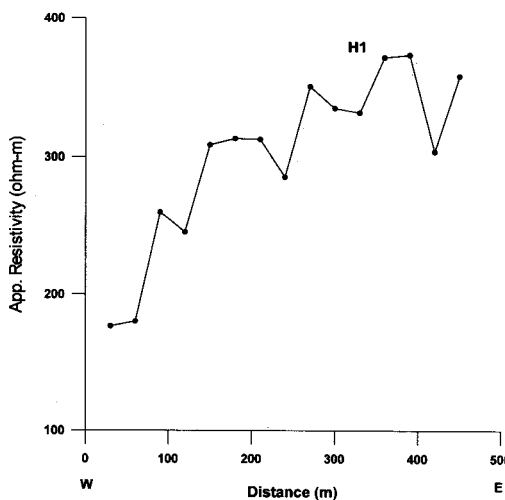

Fig. 12. Apparent resistivities of profile H1 obtained by Wenner array with electrode separation of 30 m.
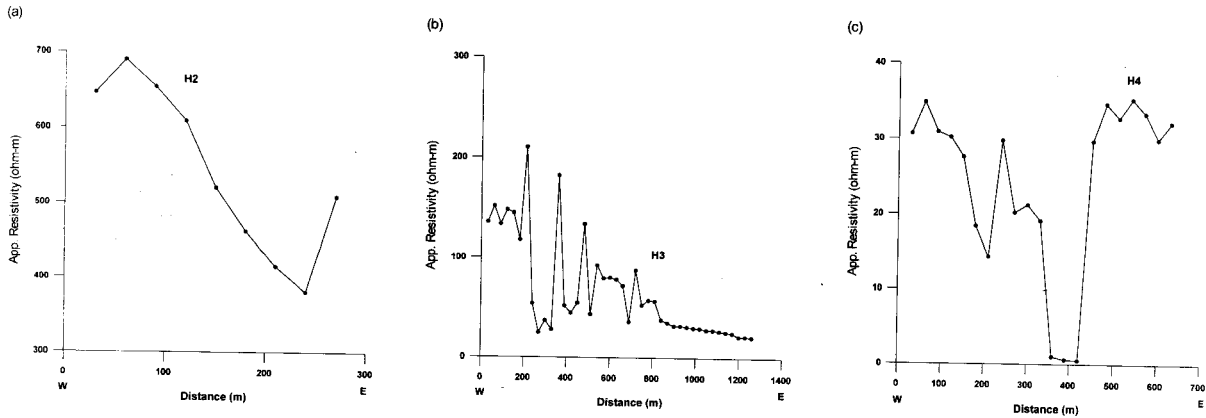
Fig. 13. Apparent resistivities of profiles H2, H3, and H4 obtained by Wenner array with electrode separation of 30 m: (a) H2, (b) H3, (c) H4.

dimensional earth and consequent interpretations in the area.

4.2. HORIZONTAL MAPPINGS

Horizontal mappings were conducted along four lines from west to east; thus, origins of Figs. 12 and 13 are near the western ends of the profiles.

Profile H1 was obtained in Ijo-ri. Fig. 12 shows that apparent resistivity of about 300-400Ωm decreases to about 100Ωm towards the inferred fault. Previous studies (Lee *et al.*, 1986; Kim · Lee, 1988; Kim *et al.*, 1990) conducted north and south of Kyeongju also reported the apparent resistivity of about 100 Ωm with the same electrode configuration of this study. Interpretations of VES V1-11 show resistivity decrease from VES V1-6 to V7-11 in conformity with profile H1.

Profile H2 conducted near Seokgye-ri also indicates decrease of apparent resistivity towards the inferred fault (Fig. 13a). The last measurement of profile H2 shows an abrupt resistivity increase, probably due to localized high resistive materials such as gravels. High resistivity values of this area (400-700 Ωm) seem to indicate the weathered layer is rather poorly developed. Profile H3 and H4 conducted in Heuisan-ri are shown in Figs. 13b and 13c, respectively. On profile H3 unstable apparent resistivities are observed at distance

200-500 m; however, they generally decrease from 100 to 20 Ωm towards the inferred fault. There is no trend of apparent resistivity decrease on profile H4 towards the inferred fault, but very low apparent resistivity of 10-40 Ωm persists on the profile. It is probable that all measurements on H3 and H4 were taken over the fault zone, not beyond it. Very low apparent resistivity values observed in this area agree with interpretations of VES V35-43. Interpretations of horizontal mappings also indicate that resistivity of the fault zone decreases from north to south in Area II.

5. CONCLUSIONS

Geoelectric surveys in the study area of the Yangsan Fault revealed the followings.

1. Along the Yangsan Fault, the fault zone turns out to be well associated with low resistivity. The weathered layer of low resistivity value in the fault zone extends down to 50-100 m.

2. The thickness of weathered layer in the fault zone of Area I (between Ijo-ri and Seoha-ri) increase from about 50 to 100 m southwards. The weathered layer of the fault zone east of the inferred fault appears to be better developed than west.

3. The basement in Area II (between Samgam-ri

and Heuisan-ri) becomes deeper from north to south. Comparing with Area I, the weathered layer in the fault zone of Area II is more conductive and extends deeper in general.

4. Apparent resistivity in horizontal mappings decreases systematically towards the inferred fault. Profiles H3 and H4 obtained in Heuisan-ri are associated with very low apparent resistivity.

ACKNOWLEDGEMENTS

REFERENCES

Dey, A. and Morrison, H. F., 1979, Resistivity modeling for arbitrarily shaped three dimensional structures, Geophysics, 44, 753-780.

Kang, P. C., 1981, Geologic evolution of Korea and structural analysis of SEATAR Korea transect area, CCOP Technical Bulletin, 14, 31-51.

Kim, I. S. and Kim, J. Y., 1983, Electric resistivity survey in the Eonyang Fault area, south-eastern Korean Peninsula, The Journal of the Korean Institute of Mining Geology, 16, 11-18.

Kim, N. J., Kwon, Y. I., and Jin, M. S., 1971, Explanatory Text of the Geological Map of Moryang Sheet; Sheet 7021-III (1:50,000), Geological Survey of Korea.

Kim, Y. and Lee., K., 1987, A study on the structure of the Yangsan Fault in the southern part of Kyeongju, The Journal of the Korean Institute of Mining Geology, 20, 247-260.

Kim, Y. and Lee., K., 1988, A geoelectric study on the Structure of the Yangsan Fault in the south of Kyeongju, Journal of the Geological Society of Korea, 24, 47-61.

Kim, Y., Lee, K., and Seong, I. K., 1990, A geoelectric study on the structure of the Yangsan Fault, north of Kyeongju, Journal of the Geological Society of Korea, 26, 393-403.

Lee, K., Cheon, K., and Um, C. R., 1992, Geoelectric surveys of the Dongrae Fault, the Eonyang Fault and the Ilkwang Fault: geophysical studies on major faults in the Kyeongsang basin, Journal of the Geological Society of Korea, 28, 218-226.

Lee, K., Jeong, B., and Kim., Y., 1985, A geophysical study of the Yangsan Fault area (II), Journal of the Geological Society of Korea, 21, 79-89.

Lee, K. and Jin, Y. G., 1991, Segmentation of the Yangsan Fault System: geophysical studies on major faults in the Kyeongsang basin, Journal of the Geological Society of Korea, 27, 434-449.

Lee, K., Kim, K. H., and Chang, T. W., 1986, Seismicity of the Korea Peninsula (II) : seismicity of the northern part of the Yangsan Fault, Journal of the Geological Society of Korea, 22, 347-365.

Lee, K. and Lee, J. H., 1997, Geoelectric study on the probable seismic segment boundaries of Yangsan Fault zone, Geoscience Journal, 1, 16-25.

Lee, K. and Na, S. H., 1983, A study of microearthquake activity along the Yangsan Fault, Journal of the Geological Society of Korea, 19, 127-135.

Lee, K. and Um, C. R., 1992, Geoelectric survey of the Ulsan Fault: geophysical studies on the major faults in the Kyeongsang basin, Journal of the Geological Society of Korea, 28, 32-39.

Lee, K. and Yoon, J. R., 1997, Numerical modeling of 3-D resistivity structures using finite difference method (in Korean): 52th Annual Meeting, The Geological Society of Korea, Abstracts, 55-56.

Lee, M. S. and Kang, P. J., 1964, Explanatory Text of the Geological Map of Yangsan Sheet; Sheet 7020-III (1:50,000), Geological Survey of Korea.

Lee, Y. J. and Lee, I. K., 1972, Explanatory Text of the Geological Map of Eon Yang Sheet; Sheet 7020-IV (1:50,000), Geological Survey of Korea.

Olorunfemi, M. O., Olarewaju, V. O., and Avci, M., 1986, Geophysical investigation of a fault zone-case history from Ile-Ife, southwest Nigeria, Geophysical prospecting, 34, 1277-1284.

Son, C. M., Lee, S. M., Kim, Y. K., Kim, S. W., and Kim, H. S., 1978, Explanatory Text of the Geological Map of Dongrae and Weolnae Sheets; Sheet 7019-IV, I (1:50,000), Korea Research Institute of Geoscience and Mineral Resources.

Ward, S. H., 1990, Resistivity and induced polarization methods: in S. H. Ward, Ed., Geotechnical and Environmental Geophysics, Volume 1: Review and Tutorial. Society of Exploration Geophysicists, 147-189.

Zohdy, A. A. R., 1989, A new method for the automatic interpretation of Schlumberger and Wenner sounding curves, Geophysics, 54, 245-253.